Nuclear Materials and Energy 42 (2025) 101885

Contents lists available at ScienceDirect

Nuclear Materials and Energy

journal homepage: www.elsevier.com/locate/nme

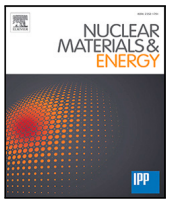

Boundary plasma studies for a spherical tokamak with lithium walls

A. Antony [a,*], L. Carbajal [a], T.D. Rognlien [b], M.V. Umansky [b], A. Froese [a], S. Howard [a], C. Ribeiro [a], R. Ivanov [a], C. Dunlea [a], C.P. McNally [a]

[a] General Fusion, 6020 Russ Baker Way, Richmond, V7B 1B4, BC, Canada
[b] Lawrence Livermore National Laboratory, Livermore, 94551, CA, USA

ARTICLE INFO

Keywords:
Plasma-surface interaction
Divertor
Limiter
Heat flux
Magnetised target fusion

ABSTRACT

Boundary plasma and plasma-material interactions are investigated for magnetised target fusion (MTF) applications. The General Fusion magnetised target fusion technology uses coaxial helicity injection (CHI) start-up which forms a spherical tokamak in a cavity with liquid lithium walls that will subsequently be compressed to fusion conditions Laberge, J. Fusion Energy (2019) The Plasma Injector 3 (PI3) experiment at General Fusion is a non-compressing experiment with solid lithium walls that studies the formation and quasi-steady state operation of a CHI spherical tokamak Carbajal et al. (2023). An explorative study is carried out for wall-limited versus diverted configurations for PI3 using the fluid edge transport code UEDGE. Experimental edge temperature and density profiles from triple Langmuir probes are used to establish realistic temperature and density profiles in UEDGE Rognlien et al. (1992) by adjusting the transport coefficients. In UEDGE, we model the wall-limited plasma via a thin limiter with various insertion depths. It is found that limiter depth and location are key parameters in determining radial profiles and sputtered lithium behaviour. Furthermore, it is found that the total sputtering of the limiter is significantly lower than the sputtering of the wall in some of the limiter configurations studied. Lithium ions and neutral behaviour are compared between limited and diverted configurations.

1. Introduction

General Fusion creates spherical tokamak (ST) target plasmas using the third generation of its coaxial helicity injector, PI3, to study the stability and confinement of ST target in the presence of solid lithium coated walls [1].

Early theoretical and numerical studies on the use of solid and liquid lithium as the first wall of standard magnetised confinement fusion (MCF) devices suggested that lithium walls would provide benefits such as more stable plasmas with higher and flatter electron and ion temperature profiles in the core plasma [2,3] due to the low recycling of hydrogenic neutrals from the lithium walls. This has been experimentally observed in various experimental fusion devices, such as in the NSTX spherical tokamak that used lithium-coated graphite walls [4–6], the LTX tokamak that used solid and liquid lithium walls [7,8], and the EAST tokamak that used solid lithium walls, puffed lithium powder into the plasma [9,10] and performed extensive studies on a liquid lithium limiter [10,11].

Modelling and simulation of lithium transport in fusion plasmas include the use of codes that solve the local neoclassical transport of impurities given a background plasma and transport coefficients [12,13] such as NCLASS [14], NEO [15], and MIST [16] that solve for the impurity profiles including atomic processes of ionisation and recombination, MHD and edge codes such as EMC3 [17], UEDGE [18], and SOLPS [19] that solve the background plasma (main hydrogenic ions and electrons) and use either a fluid description for impurities that evolves consistently with the background plasma or a kinetic description of impurities through coupling to codes such as EIRENE [20] or DEGAS2 [21] that solve for the guiding-centre orbits of impurities including atomic physics and collisions with the background plasma. More detailed modelling and simulation of the transport of other impurities, such as carbon, in fusion experiments solve for the drift-kinetic dynamics of the main hydrogenic ions, electrons, and impurities, allowing the inclusion of anomalous transport coefficients. Examples of this type of modelling are the XGC0 and XGC1 codes [12,22]. However, it is noted that this latter approach may result in very expensive simulations that prevent the extensive application of this approach.

PI3 routinely operates in a magnetic configuration where particle and heat fluxes from the core will deposit to divertor and inboard limiter surfaces. This allows for exploring the effects of fluxes to multiple surfaces on edge and plasma performance concerning neutral and

* Corresponding author.
E-mail address: abetharan.antony@generalfusion.com (A. Antony).

https://doi.org/10.1016/j.nme.2025.101885
Received 17 May 2024; Received in revised form 28 October 2024; Accepted 24 January 2025
Available online 31 January 2025

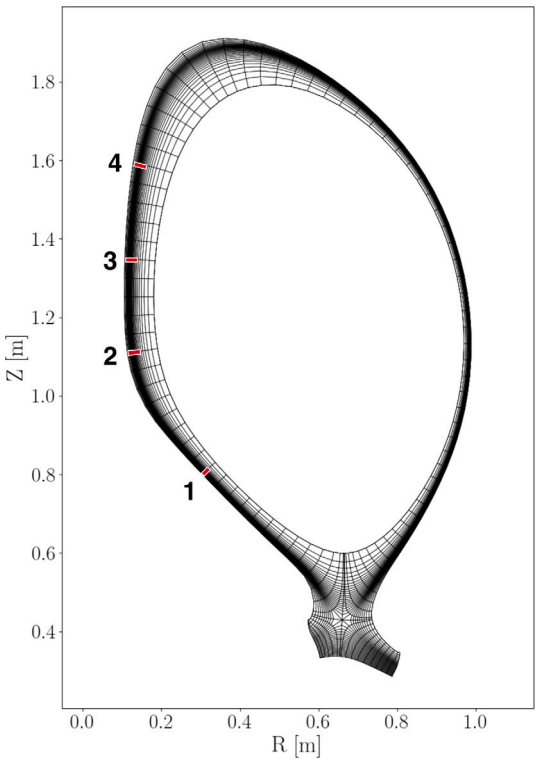

Fig. 1. UEDGE mesh utilised for this study. Mesh refinement was not applied. Locations of the limiter are highlighted for the four poloidal locations studied.

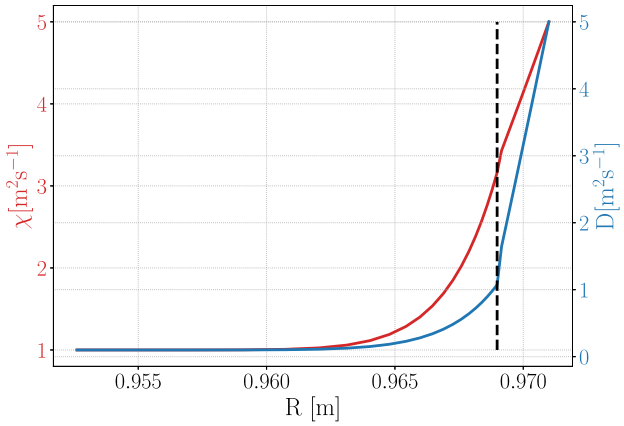

Fig. 2. Transport coefficients used in this study shown at the outer midplane, with the separatrix highlighted with a dashed line.

lithium impurity behaviour. This is not an operating mode unique to PI3, but also occurs in tokamaks, where particle and heat fluxes will impact various surfaces such as the centre-post and baffles near the x-point whilst simultaneously being diverted.

To model this, we insert a thin plate limiter in a divertor configuration and examine the edge behaviour. We study the impact of various plasma configurations in PI3 ranging from diverted configurations to multiple scenarios with a thin plate limiter that are possibly expected on PI3 and indeed on other tokamaks of equivalent size using the edge code UEDGE [18]. This study provides valuable information for understanding typical edge behaviour resulting from fluxes depositing on limiter and divertor surfaces in the presence of lithium-coated walls. We present three separate studies: (1) Limiter insertion depth effect, (2) The impact of limiter location and (3) Purely diverted compared with limited inboard operation. Finally, we present early design studies for a plasma compression device.

2. Simulation setup

We utilise the edge code UEDGE to solve the 2D fluid equations for the hydrogenic and impurity species. The impurity momentum equations are solved with an assumption of force balance and are flux-limited in the radial and poloidal directions. Furthermore, parallel thermal transport is flux-limited. Additional details of the equations solved can be found in [18,23]. Recently recommissioned UEDGE features are utilised in this work:

- Thin Plate Limiters
- Evaporation from Limiter
- Sputtering from Limiter

In addition to the thin plate limiter, UEDGE has recently been upgraded to include the interaction of impurities on a radial limiter inserted radially at some poloidal position. In this work, physical sputtering by deuterium ions incident on the limiter injects lithium neutrals into the plasma volume. The sputtering coefficients are taken from Eckstein [24].

UEDGE is used to find a steady state solution for PI3 shot #18447 at $t = 5\,\text{ms}$. This specific time is typically the most quiescent period for plasmas in PI3, after which an approximation of steady state would fail. We set up our field-aligned mesh based on PI3 #18447 (Fig. 1) with the mesh extending in ψ_{norm} from 0.925 to 1.011 utilising a Grad–Shafranov (GS) equilibrium generated with CORSICA [25] based on experimental data. We utilise 45 and 30 cells poloidally (inboard and outboard respectively) as well as 30 cells radially. For limited configurations, we refine the mesh around the limiter to reach a resolution of $\Delta x_{\text{guard}} < 5\,\mu\text{m}$.

A density of $n_{\text{core}} = 1.84 \times 10^{19}\,\text{m}^{-3}$, which is inferred from interferometers, is imposed at the core boundary. In addition, we specify the density gradient scale length to the walls which is set to $L_{D+} = 0.01\,\text{m}$. We used fixed temperature boundary conditions of $T_e^{\text{inner}} = 24\,\text{eV}$ and $T_e^{\text{outer}} = 4\,\text{eV}$ informed by Langmuir probe measurements and from these set the T_i boundary values by an assumption of $T_i \sim 1.3T_e$ inspired by ion Doppler spectroscopy measurements. Field lines in contact with material surfaces, such as the divertor plates or limiter, are subject to sheath boundary conditions with conservative heat transmission coefficients of $\gamma_e = 4.0$ for electrons and $\gamma_i = 2.5$ for ions.

A modest recycling coefficient $R = 0.75$ is used for deuterium, which is higher than the expected recycling coefficient of $R \sim 0.5$ reported in LTX-β [26]. However, PI3 discharge 18447 was performed with worn lithium (30 shots after evaporative coating) and thus, we expect the lithium to be significantly passivated and lithium coating variability to be significant. Therefore, we take a conservative estimate of the recycling coefficients in these simulations. We utilise a recycling coefficient of $R = 0$ for lithium i.e. any ionised lithium that strikes any material surface is effectively absorbed. Evaporation off all surfaces is included. The surface temperature of the walls is set to 293 K and the limiter to 310 K. These low temperatures produce small evaporation rates, but they are included for completeness. We expect the limiter to become hotter due to heat fluxes from the plasma during transient pulses. However, since the heat fluxes are experimentally unknown, a key part of this study involves theoretically calculating the expected heat loads experienced by the limiter and divertor.

We specify spatially dependent particle diffusivity D and electron thermal diffusivity χ_e. The ion thermal diffusivity is set to the electron value ($\chi_i = \chi_e$). In this study, we utilise the profile shown in Fig. 2 in an attempt to match the Langmuir probe data at the outer mid-plane. This data is only available at one poloidal location, so we do not attempt to match any poloidal variation. As seen in Fig. 3, we find a good matching of the temperature and density profiles from the Langmuir probe, where Langmuir probe data is collected over multiple shots at

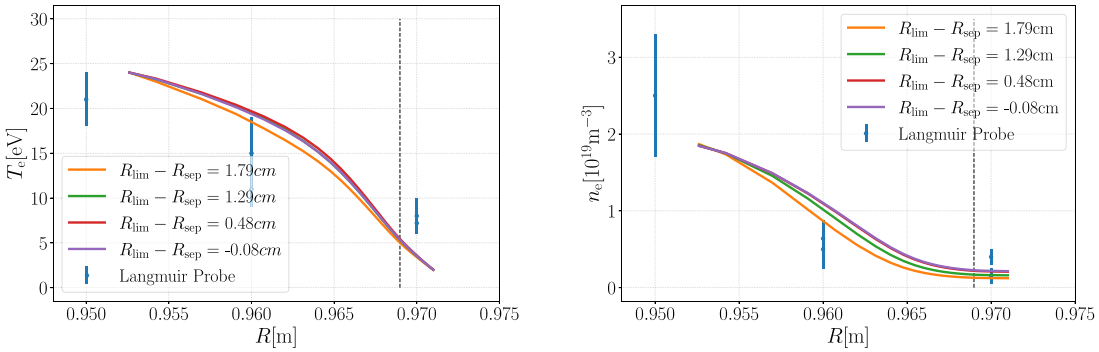

Fig. 3. Comparison of three limiter insertion depths compared to measured Langmuir probes data. The separatrix is highlighted with a dashed line, with the edge region left of the separatrix and the SOL to the right, *left*: Electron temperature and *right*: Density.

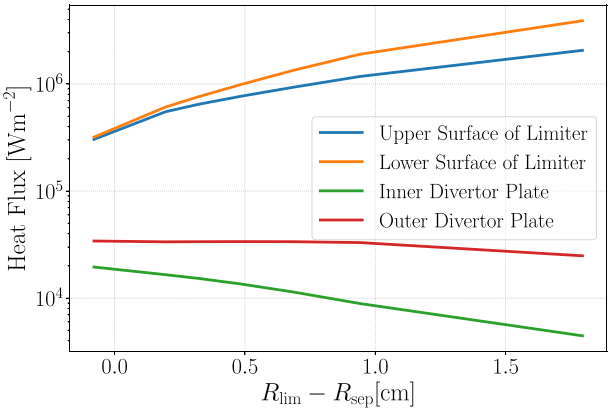

Fig. 4. Heat fluxes to the limiter and divertor plates compared with limiter insertion depth.

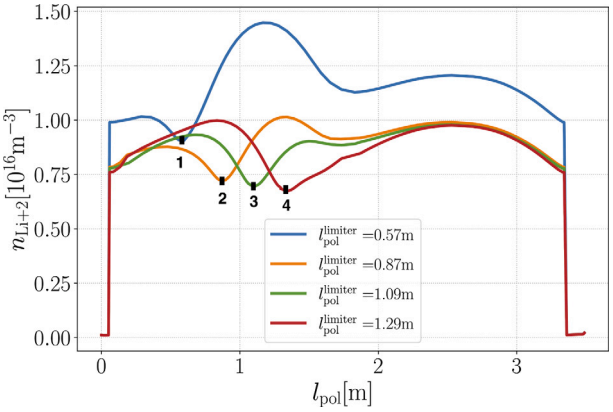

Fig. 5. Li+2 density along the magnetic surface 6 cells from the separatrix. The black squares indicate the location of the limiter and the numbers correspond to limiter positions in Fig. 1. l_{pol} is the length from the inner divertor plate to the outer.

similar settings (#18660–#18669). Shot-to-shot variation is expected, and thus, the discrepancy observed between UEDGE and the Langmuir probe data is within the uncertainty of the experimental data. It is noted that the SOL transport coefficients in this model are the same order as Bohm diffusion (~3 m^2s^{-1}) [27].

3. Results and discussion

The first study compares insertion depth and its effects on the heat fluxes on the limiter and divertor surfaces. Previous work by Rensink and Rognlien [28] showed a clear inverse trend with respect to the insertion depth and heat flux to the divertor plates with an outboard limiter inserted. In this work, we insert the limiter on the inboard side with insertion depth varying from $R_{lim} - R_{sep} = -0.08$ to 1.79 cm, where $R_{lim} - R_{sep}$ is the insertion depth relative to the separatrix. In this case $R_{lim} - R_{sep} < 0$ cm indicates that the limiter is inserted into the SOL and $R_{lim} - R_{sep} > 0$ cm within the separatrix. We find a similar trend to Rensink and Rognlien [28] as shown in Fig. 4. Sufficient retraction of the limiter was not performed, and thus the crossing point discussed in [28] is not seen.

Notably, in these simulations, inserting the limiter tip just beyond the last closed flux surface (LCFS) has little effect on both the wall heat flux and the divertor heat flux, as shown in Table 1. In these instances, the particle flux to the limiter is sufficiently low, resulting in modest effects on the overall dynamics of the simulation. Consequently, the heat fluxes and particle fluxes to the wall and divertor remain qualitatively unaffected. In addition, the limiter experiences sheath heat fluxes with temperatures and densities close to core plasma values, leading, in some cases, to significantly higher heat fluxes on the limiter than those observed on the wall.

However, a notable difference between this study and the work of Rensink and Rognlien [28] is the occurrence of reduced limiter pumping. It is easily seen in Fig. 3 that at the furthest insertion at $R_{lim} - R_{sep} = 1.79$ cm there is a small difference in the density profile. However, it is not as dominant an effect as previously reported. In these simulations, the wall acts as the largest recycling surface, until the limiter dominates at an insertion depth of $R_{lim} - R_{sep} > 1.64$ cm, where the limiter affects the density profile. Some effects are observed as early as $R_{lim} - R_{sep} = 1.29$ cm but the wall remains the pumping surface from which deuterium ions interact and recycle. This can also be seen comparing the deuterium ion fluxes interacting with the limiter at $R_{lim} - R_{sep} = 0.2$ cm, where the limiter current is 19 A and the wall current is 196 A with other particle fluxes shown in Table 1. As both surfaces have the same recycling coefficient, the density profile is dominated by wall dynamics and not limiter pumping in these instances.

Furthermore, the sputtered lithium transitions from being predominantly sourced from the wall to the limiter as the limiter is inserted further towards the core region. The limiter pumps lithium in the instances of the wall being the source of lithium, and as the limiter is more deeply inserted all material surfaces become important sources of lithium. This can be understood via a comparison of neutral lithium current from the wall/limiter for two separate limiter insertions, where a more negative current indicates a greater net flux of lithium moving away from the limiter. At $R_{lim} - R_{sep} = 0.1$ cm the neutral currents are −0.21 A / −0.1 A, where almost double the lithium is coming from the walls. However, at $R_{lim} - R_{sep} = 1.5$ cm the currents are −0.1 A / −3.2 A — a 32 times difference. This is a result from the leading edge being immersed in high energy particles resulting in higher sputtering yield and a larger wetted area.

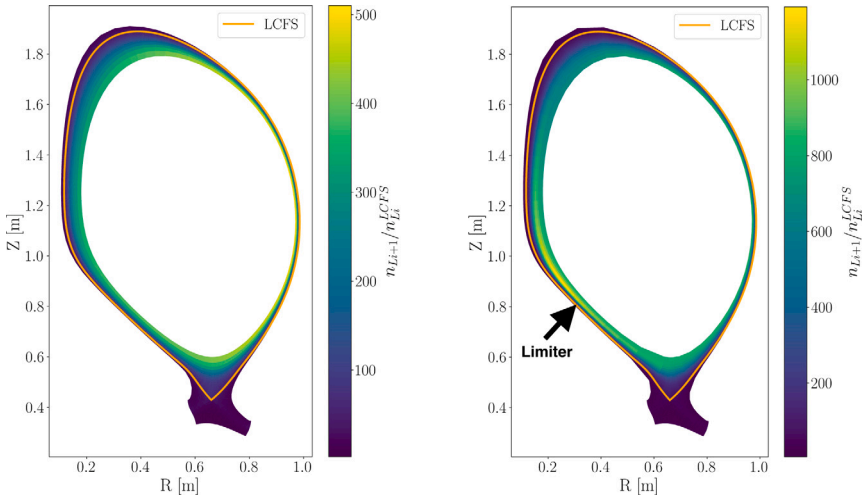

Fig. 6. Li + 1 density normalised to neural lithium at the LCFS with *left*: Diverted and *right*: Limited plasmas.

Table 1
Deuterium particle fluxes and total heat fluxes on various surfaces in different limiter settings and purely divertor configuration. The divertor and limiter fluxes are summed for simplicity.

	Particle flux/A			Heat flux/MWm^{-2}		
	Wall	Divertor	Limiter	Wall	Divertor	Limiter
Diverted	216	28	–	0.25	0.10	–
$R_{lim} - R_{sep} = -.08$ cm	202	24	11	0.25	0.05	0.6
$R_{lim} - R_{sep} = 0.48$ cm	186	20	30	0.22	0.05	1.8
$R_{lim} - R_{sep} = 1.29$ cm	132	15	106	0.26	0.04	4.3
$R_{lim} - R_{sep} = 1.79$ cm	90	12	191	0.40	0.03	6.0

The second study compares the location of the limiter as varying from position 1 to 4 in Fig. 1 with the limiter inserted into the same flux surfaces. We find that there is poloidal variation in impurity species density as would be expected. We see in Fig. 5 that Li + 2 has a strong dependence on the limiter location in the plasma. This is the case for all ion species of lithium. The poloidal position (l_{pol}) of the limiter is indicated in these plots by the drop in density as sputtered lithium is primarily neutral or singly ionised near the limiter.

Due to the limiter being on the same flux surface as its position is moved poloidally in the UEDGE mesh, the physical area of the limiter increases as it moves from position 1 to 4 shown in Fig. 1. Further away from the private flux region (position 4) the limiter has the largest wetted area, decreasing as it moves towards the divertor. This results in the limiter locations having a significant impact on the magnitude of the ionised lithium density. Partly due to parts of the limiter acting to absorb the ionised lithium in the simulation as the recycling coefficient is effectively zero on all surfaces for lithium. Effects resulting from changes in the deuterium density due to limiter pumping will also affect lithium concentration owing to changes in sputtering yield. Thus, a limiter closer to the private flux region results in larger concentration of lithium in the plasma as opposed to a limiter beyond the inner mid-plane.

The final study carried out compares a diverted plasma with no limiter to one with a limiter inserted at position 1 in Fig. 1 and insertion depth of $R_{lim} - R_{sep} = 0.48$ cm. Of primary interest is how the heat-fluxes to the various surfaces differ, as well as the behaviour of the impurities and neutrals. It is expected that the heat-flux on the divertor plate closest to the limiter will be significantly lower as seen in the previous study. Indeed, the limiter reduces the heat-flux to the left divertor plate by 62% and the right divertor plate by 40%.

The diverted configuration has an impurity concentration of 1% compared to the limiter configuration, which has a concentration of ∼0.3%. Both configurations do not have a detrimental amount of lithium ions present [29]. Nevertheless, in denser and higher-power machines, impurity concentrations are expected to increase, making it crucial to understand the impact of this difference. In both configurations, the wall serves as a significant source of impurities from physical sputtering due to a main ion flux of $\mathcal{O}(10^2)$ A. However, in the limiter case, the limiter surface in the SOL helps reduce deuterium density and lowers the temperature. As a result, the main ion flux to the wall decreases, leading to a reduction in the overall sputtered yield from the walls, which in turn reduces the total lithium concentration in the SOL region. Furthermore, part of the limiter acts as a net sink for lithium, further lowering the overall lithium levels in the SOL. This is illustrated by the low-density region of singly ionised lithium in Fig. 6, where the entire low-density area corresponds to the extent of the limiter. At the leading edge of the limiter, there is a net source of lithium, as indicated by the localised increase in ionised lithium concentration at the limiter's position.

Finally, we highlight ongoing work utilising an outboard thin limiter in early design work on a future device for compressing spherical tokamak plasmas shown in Fig. 7. In this study, we used an outboard limiter under the assumption that the compressing wall limits the plasma. These models exploit the ability of UEDGE to model an up-down symmetric double-null configuration as a half-domain using a symmetric boundary condition at the equator. The limiter is located at $Z \sim 0.65$ m near the symmetry plane with an insertion depth of $R_{lim} - R_{sep} = -0.25$ cm, which in this case is 0.25 cm into the core region. Expected lithium behaviour is observed in Fig. 7, with a maxima local to the limiter tip. This suggests that the limiter application is physically reasonable in this novel geometry as well, and future design studies can be carried out to minimise lithium ingress using a limiter.

4. Summary and conclusions

The first edge plasma calculations of PI3 have been conducted in the regime of a diverted plasma and with a limiter inserted, in the presence of solid lithium surfaces. We find that limiter insertion depth is a key parameter in determining heat fluxes to the divertor plates. As the limiter is inserted past the separatrix, the heat fluxes to the limiter increases and the divertor heat fluxes decreases in agreement with previous work [28]. The primary particle fluxes in this case are directed towards the walls, which serve as the primary pumping surface. This is unlike what is reported in [28] where a large impact on the density profile is observed even for modest limiter insertion, a behaviour that is found in this work only after deep insertion of the limiter. That study [28] effectively used a unity wall recycling, but a limiter with $R = 0.8$, which we attribute the difference to.

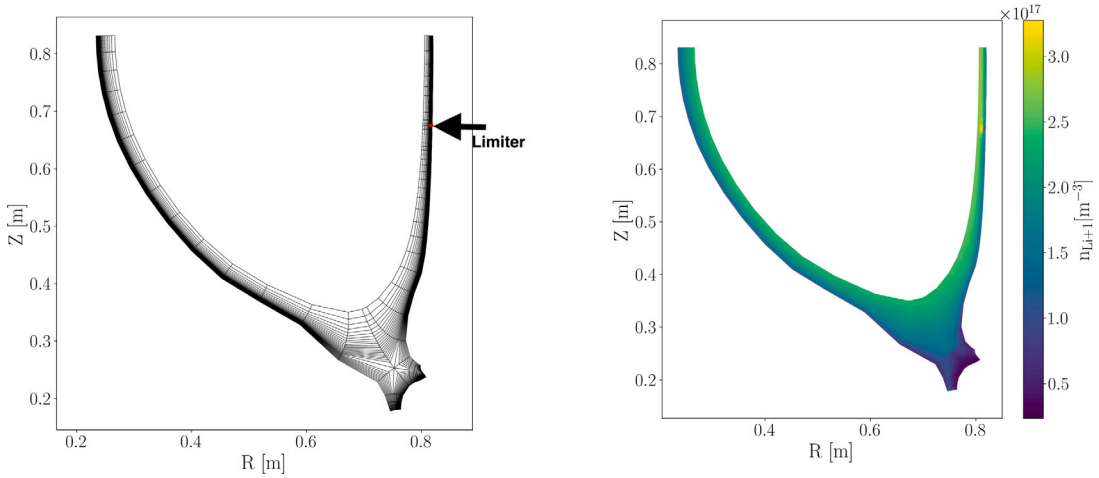

Fig. 7. *left*: Mesh for a design stufy of a next-generation plasma compression device in the pre-compressed state mesh with limiter highlighted in red and *right*: Li + 1 density. (For interpretation of the references to colour in this figure legend, the reader is referred to the web version of this article.)

In addition, we find that the location of the limiter determines the impurity distribution. As the limiter is moved away from the private flux region the impurity densities reduce due to changes in the plasma wetted area seen by the plasma. At position 4, the wetted area is the largest and therefore results in a reduction in lithium as the limiter due to a reduction in sputtering yield as well as parts of the limiter acting as sink. This trend continues in an anti-clockwise direction with increasing lithium concentration. Furthermore, it is found that the insertion of the limiter compared to a fully diverted plasma causes a reduction of heat fluxes by 62% and 40% to the inner and outer divertor plates. However, the diverted plasmas have significantly more impurities present due to the wall being a large source of impurities with no sinks near the core plasma. Whereas, the limiter acts to decrease lithium density via reducing the deuterium density in the SOL resulting in a decreased sputtering yield. In addition, the limiter acts as a sink on parts of it surfaces to lithium reducing the overall lithium in the plasma further.

Finally, we highlight the use of a thin limiter on the outboard side for a novel device currently being designed. The outboard limiter results in physically reasonable behaviour suggesting that UEDGE is capable and applicable for future design studies of the plasma compression device.

Future work involves utilising more accurate boundary conditions representing the power entering the plasma. In addition, exploring the effects of the recycling coefficient and how that affects the edge region is of interest. The final aim is to extend this modelling to a compressing spherical tokamak design study.

CRediT authorship contribution statement

A. Antony: Writing – original draft, Visualization, Methodology, Investigation, Formal analysis, Conceptualization. **L. Carbajal:** Writing – review & editing, Software, Methodology. **T.D. Rognlien:** Writing – review & editing, Supervision, Software, Methodology, Conceptualization. **M.V. Umansky:** Writing – review & editing, Supervision, Software, Conceptualization. **A. Froese:** Writing – review & editing, Resources. **S. Howard:** Writing – review & editing, Resources. **C. Ribeiro:** Resources. **R. Ivanov:** Resources. **C. Dunlea:** Resources. **C.P. McNally:** Writing – review & editing, Supervision.

Declaration of competing interest

The authors declare that they have no known competing financial interests or personal relationships that could have appeared to influence the work reported in this paper.

Acknowledgements

We thank the experimental group at General Fusion for the experimental results. Performed in part by LLNL under Contract DE-AC52-07NA27344 in support of General Fusion under SPP-L23083. This work was supported by funding from the Government of Canada through its Strategic Innovation Fund (Agreement No. 811-811346). The funding source had no involvement in: the study design; the collection, analysis and interpretation of data; the writing of the report; the decision to submit the article for publication.

Data availability

Data will be made available on request.

References

[1] A. Tancetti, C. Ribeiro, S.J. Howard, S. Coop, C.P. McNally, M. Reynolds, P. Kholodov, F. Braglia, R. Zindler, C. Macdonald, E. Love, P. Carle, X. Feng, A. Rohollahi, K. Leci, D. Plant, C. Dunlea, R. Ivanov, A. Mossman, Thermal energy confinement time of spherical tokamak plasmas in PI3, Nucl. Fusion (2024) In review.

[2] S.I. Krasheninnikov, L.E. Zakharov, G.V. Pereverzev, On lithium walls and the performance of magnetic fusion devices, Phys. Plasmas 10 (2003) 1678–1682, http://dx.doi.org/10.1063/1.1558293.

[3] T.D. Rognlien, M.E. Rensink, Impurity transport in edge plasmas with application to liquid walls, Phys. Plasmas 9 (5) (2002) 2120–2126, http://dx.doi.org/10.1063/1.1461384.

[4] M.G. Bell, H.W. Kugel, R. Kaita, L.E. Zakharov, H. Schneider, B.P. Leblanc, D. Mansfield, R.E. Bell, R. Maingi, S. Ding, S.M. Kaye, S.F. Paul, S.P. Gerhardt, J.M. Canik, J.C. Hosea, G. Taylor, Plasma response to lithium-coated plasma-facing components in the national spherical torus experiment, Plasma Phys. Control. Fusion 51 (12) (2009) http://dx.doi.org/10.1088/0741-3335/51/12/124054.

[5] J.M. Canik, R. Maingi, S. Kubota, Y. Ren, R.E. Bell, J.D. Callen, W. Guttenfelder, H.W. Kugel, B.P. Leblanc, T.H. Osborne, V.A. Soukhanovskii, Edge transport and turbulence reduction with lithium coated plasma facing components in the national spherical torus experiment, Phys. Plasmas 18 (5) (2011) http://dx.doi.org/10.1063/1.3592519.

[6] R. Maingi, J.M. Canik, R.E. Bell, D.P. Boyle, A. Diallo, R. Kaita, S.M. Kaye, B.P. LeBlanc, S.A. Sabbagh, F. Scotti, V.A. Soukhanovskii, Effect of progressively increasing lithium conditioning on edge transport and stability in high triangularity NSTX H-modes, Fusion Eng. Des. 117 (2017) 150–156, http://dx.doi.org/10.1016/j.fusengdes.2016.06.058.

[7] R. Majeski, R.E. Bell, D.P. Boyle, R. Kaita, T. Kozub, B.P. LeBlanc, M. Lucia, R. Maingi, E. Merino, Y. Raitses, J.C. Schmitt, J.P. Allain, F. Bedoya, J. Bialek, T.M. Biewer, J.M. Canik, L. Buzi, B.E. Koel, M.I. Patino, A.M. Capece, C. Hansen, T. Jarboe, S. Kubota, W.A. Peebles, K. Tritz, Compatibility of lithium plasma-facing surfaces with high edge temperatures in the lithium tokamak experiment, Phys. Plasmas 24 (2017) 056110, http://dx.doi.org/10.1063/1.4977916.

[8] D.P. Boyle, R. Majeski, J.C. Schmitt, C. Hansen, R. Kaita, S. Kubota, M. Lucia, T.D. Rognlien, Observation of flat electron temperature profiles in the lithium tokamak experiment, Phys. Rev. Lett. 119 (2017) http://dx.doi.org/10.1103/PhysRevLett.119.015001.

[9] G.Z. Zuo, J.S. Hu, J.G. Li, Z. Sun, D.K. Mansfield, L.E. Zakharov, Lithium coating for H-mode and high performance plasmas on EAST in ASIPP, J. Nucl. Mater. 438 (SUPPL) (2013) 90–95, http://dx.doi.org/10.1016/j.jnucmat.2013.01.014.

[10] T. Xie, S.Y. Dai, G.Z. Zuo, L. Wang, H.M. Zhang, B. Lyu, L. Zhang, J. Huang, J.S. Hu, Y. Feng, D.Z. Wang, EMC3-EIRENE modelling of edge plasma and impurity emissions compared with the liquid lithium limiter experiment on EAST, Nucl. Fusion 58 (10) (2018) 106017, http://dx.doi.org/10.1088/1741-4326/aad42f.

[11] T. Xie, S.Y. Dai, Z. Sun, G.Z. Zuo, J.S. Hu, Y. Feng, D.Z. Wang, Investigation of edge impurity transport and divertor fluxes by toroidally localized lithium injection on EAST with EMC3-EIRENE, Plasma Phys. Control. Fusion 61 (11) (2019) http://dx.doi.org/10.1088/1361-6587/ab434a.

[12] F. Scotti, V.A. Soukhanovskii, R.E. Bell, S. Gerhardt, W. Guttenfelder, S. Kaye, R. Andre, A. Diallo, R. Kaita, B.P. Leblanc, M. Podestá, Core transport of lithium and carbon in ELM-free discharges with lithium wall conditioning in NSTX, Nucl. Fusion 53 (2013) http://dx.doi.org/10.1088/0029-5515/53/8/083001.

[13] D.P. Boyle, Measurements of Impurity Concentrations and Transport in the Lithium Tokamak Experiment (Ph.D. thesis), Princeton University: Plasma Physics Department, 2016.

[14] W.A. Houlberg, K.C. Shaing, S.P. Hirshman, M.C. Zarnstorff, Bootstrap current and neoclassical transport in tokamaks of arbitrary collisionality and aspect ratio, Phys. Plasmas 4 (9) (1997) 3230–3242, http://dx.doi.org/10.1063/1.872465, arXiv:https://doi.org/10.1063/1.87246.

[15] E.A. Belli, J. Candy, Kinetic calculation of neoclassical transport including self-consistent electron and impurity dynamics, Plasma Phys. Control. Fusion 50 (9) (2008) 095010, http://dx.doi.org/10.1088/0741-3335/50/9/095010.

[16] R.A. Hulse, Numerical studies of impurities in fusion plasmas, Nucl. Technol. Fusion 3 (2) (1983) 259–272, http://dx.doi.org/10.13182/FST83-A20849, arXiv:https://doi.org/10.13182/FST83-A20849.

[17] J. Lore, J. Canik, Y. Feng, J.-W. Ahn, R. Maingi, V. Soukhanovskii, Implementation of the 3D edge plasma code EMC3-EIRENE on NSTX, Nucl. Fusion 52 (5) (2012) 054012, http://dx.doi.org/10.1088/0029-5515/52/5/054012.

[18] T. Rognlien, J. Milovich, M. Rensink, G. Porter, A fully implicit, time dependent 2-D fluid code for modeling tokamak edge plasmas, J. Nucl. Mater. 196–198 (1992) 347–351, http://dx.doi.org/10.1016/S0022-3115(06)80058-9, URL https://www.sciencedirect.com/science/article/pii/S0022311506800589. Plasma-Surface Interactions in Controlled Fusion Devices.

[19] R. Schneider, X. Bonnin, K. Borrass, D.P. Coster, H. Kastelewicz, D. Reiter, V.A. Rozhansky, B.J. Braams, Plasma edge physics with B2-Eirene, Contrib. Plasma Phys. 46 (2006) 3–191, http://dx.doi.org/10.1002/ctpp.200610001.

[20] D. Reiter, M. Baelmans, P. Börner, The EIRENE and B2-EIRENE codes, Fusion Sci. Technol. 47 (2) (2005) 172–186, http://dx.doi.org/10.13182/FST47-172.

[21] D. Stotler, C. Karney, Neutral gas transport modeling with DEGAS 2, Contrib. Plasma Phys. 34 (2–3) (1994) 392–397, http://dx.doi.org/10.1002/ctpp.2150340246, arXiv:https://onlinelibrary.wiley.com/doi/pdf/10.1002/ctpp.2150340246.

[22] D.J. Battaglia, K.H. Burrell, C.S. Chang, S. Ku, J.S. Degrassie, B.A. Grierson, Kinetic neoclassical transport in the H-mode pedestal, Phys. Plasmas 21 (7) (2014) http://dx.doi.org/10.1063/1.4886803.

[23] T.D. Rognlien, D.D. Ryutov, N. Mattor, G.D. Porter, Two-dimensional electric fields and drifts near the magnetic separatrix in divertor tokamaks, Phys. Plasmas 6 (5 I) (1999) 1851–1857, http://dx.doi.org/10.1063/1.873488.

[24] W. Eckstein, Physical sputtering and reflection processes in plasma-wall interactions, J. Nucl. Mater. 248 (1997) 1–8, http://dx.doi.org/10.1016/S0022-3115(97)00109-8, URL https://www.sciencedirect.com/science/article/pii/S0022311597001098.

[25] J. Crotinger, L. LoDestro, L. Pearlstein, A. Tarditi, T. Casper, E. Hooper, LLNL Report UCRL-ID-126284, NTIS# PB2005-102154, 1997.

[26] A. Maan, D.P. Boyle, R. Majeski, G.J. Wilkie, M. Francisquez, S. Banerjee, R. Kaita, R. Maingi, B.P. LeBlanc, S. Abe, E. Jung, E. Perez, W. Capecchi, E.T. Ostrowski, D.B. Elliott, C. Hansen, S. Kubota, V. Soukhanovskii, L. Zakharov, Estimates of global recycling coefficients for LTX-β discharges, Phys. Plasmas 31 (2) (2024) 022505, http://dx.doi.org/10.1063/5.0177604, arXiv:https://pubs.aip.org/aip/pop/article-pdf/doi/10.1063/5.0177604/19676596/022505_1_5.0177604.pdf.

[27] M.S. Islam, J.D. Lore, C. Lau, J. Rapp, Analysing the effects of heating and gas puffing in proto-MPEX helicon and auxiliary heated plasmas, Plasma Phys. Control. Fusion 65 (9) (2023) 095020, http://dx.doi.org/10.1088/1361-6587/ace793.

[28] M. Rensink, T. Rognlien, Edge plasma modeling of limiter surfaces in a tokamak divertor configuration, J. Nucl. Mater. 266–269 (1999) 1180–1184, http://dx.doi.org/10.1016/S0022-3115(98)00859-9, URL https://www.sciencedirect.com/science/article/pii/S0022311598008599.

[29] M. Islam, J. Lore, S. Smolentsev, C. Kessel, R. Maingi, Analysis and design of fast flow liquid li divertor for fusion nuclear science facility (FNSF) using coupled plasma boundary and LM MHD/heat transfer codes, Nucl. Fusion 64 (5) (2024) 056036, http://dx.doi.org/10.1088/1741-4326/ad3a7b.